Molecular Structure Analysis and Spectroscopic Properties of Monoazo Disperse Dye From *N,N*-Dimethylaniline

Ömer ARSLAN[1], Ergin YALÇIN[1], Nurgül SEFEROĞLU[2,*], Müjgan YAMAN[3], Zeynel SEFEROĞLU[1]

[1]*Department of Chemistry, Gazi University, 06500 Ankara, Turkey.*

[2]*Advanced Technologies, Gazi University, 06500 Ankara, Turkey.*

[3]*Department of Chemistry, Eskişehir Osmangazi University, 26480 Eskişehir, Turkey.*

Article Info	Abstract
	A monoazo disperse dye (DMA) was prepared by diazotizing 4-aminoacetophenone and coupling with N,N-dimetylaniline. It was fully characterized by IR, UV, ^{1}H-NMR, ^{13}C-NMR, TGA, and mass spectral techniques as well as X-ray crystallographic methods. The electronic absorption spectra of the dye in solvents of different polarities covers a λ_{max} range of 437-460 nm. It is shown that the compound exhibits positive solvatochromism in solution. In addition, the absorption properties of the compound change drastically upon acidification, as the protonation of β-nitrogen atom of the azo group increases the donor-acceptor interplay of the π system. The molecular structure, spectroscopic and nonlinear optical (NLO) properties of DMA were also investigated theoretically by performing Density Functional Theory (DFT) and Hartree–Fock (HF) levels of theory using the 6-31+G(d,p) basis set. The optimized geometries, electronic absorption spectra calculated using time-dependent DFT (TD-DFT) method and NMR spectra were evaluated via comparison with experimental values. In addition, thermal analysis shows that DMA is thermally stable up to 258 °C.

1. INTRODUCTION

Disperse dyes are the most important dyes group for dyeing of hydrophobic fibres. They have low solubility in water and are able to retain better substantivity for hydrophobic fibres, such as polyester, nylon and acetate. Azo dyes used as disperse dyes have strong tinctorial strength compared to anthraquinone dyes, ease to make, and a low cost of manufacture. The majority of commercially important disperse azo colorants contain a single azo bridge [1,2] and many of them bearing *N,N*-dialkylaniline as coupling component have been studied in the past decades [3-21] (Scheme 1). Recently, in our research group many functional azo dyes which have various spectroscopic properties have been synthesized [22-24]. Our previous work [25] prompted us to study on azo disperse dyes bearing *N,N*-dialkyl/arylaminophenyl as strong electron-donating coupling component. Therefore, in current study, we synthesized and characterized the azo dye (DMA) bearing carbonyl group in the para-position of diazo component and as coupling component of *N,N*-dimethylaniline. The structure of DMA was characterized by UV-vis, IR, ^{1}H-NMR, ^{13}C-NMR and mass spectroscopic techniques. To determine the molecular structure forms of DMA in solid state, X-ray data were recorded. Also, we investigated the influence of solvents of different polarities and acid on the UV-vis absorption spectra of the molecule. However, the structural characterization of DMA was also investigated using theoretical methods including Hartree–Fock (HF) and density functional theory (DFT) calculations. The theoretical electronic absorption spectra was calculated using TD-DFT method. Molecular hyperpolarizability was also calculated by DFT and HF methods. The ^{1}H and ^{13}C-NMR chemical shifts of DMA were determined and compared with experimental results.

*Corresponding author, e-mail: nurguls@gazi.edu.tr
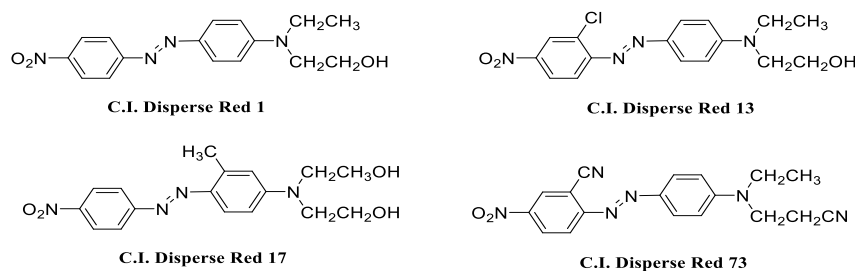
Scheme 1. *Some commercial disperse azo dyes bearing N,N-dialkylamine as coupling component.*

2. EXPERIMENTAL DETAILS

2.1. Materials and instrumentation

The chemical used in the synthesis of the compounds was procured from the Aldrich Chemical Company and used without further purification. The solvents were used of spectroscopic grade. Infrared (IR) spectra were recorded by Perkin Elmer Spectrum Two with U-ATR FT-IR spectrometer in the region 350-4000cm^{-1}. NMR spectra were recorded on a Bruker Avance 300 Ultra-Shield in DMSO-d_6. Chemical shifts are expressed in δ units (ppm). Ultraviolet-visible (UV-vis) absorption spectra were recorded on Shimadzu Corporation, Kyoto Japan UV-1800 240 V spectrophotometer at the wavelength of maximum absorption (λ$_{max}$, in nm) in the solvents specified. Mass analysis was obtained by Waters 2695 Alliance ZQ Micromass LCMS working with ESI apparatus; in m/z (rel. %) (Ankara University Laboratories, Department Pharmacological Sciences). Chemical shifts are expressed in δ units (ppm) with tetramethylsilane (TMS) as the internal reference. Coupling constant (*J*) is given in hertz (Hz). Signals are abbreviated as follows: singlet, s; doublet, d; triplet, t, multiplet, m. The melting points were measured Electrothermal IA9200 apparatus are uncorrected. Thermal analyses were performed with a Shimadzu DTG-60H system, up to 600 °C (10 °C min^{-1}) under a dynamic nitrogen atmosphere (15 mL min^{-1}).

2.2. Synthesis

DMA was prepared by coupling the reaction of *N,N*-dimethylaniline with 4-aminoacetophenone in dilute hydrochloric acid by using literature method [26] (Scheme 2). The structure of the prepared dye has been confirmed by IR, UV-vis, ^{1}H-NMR, ^{13}C-NMR, LC-MS and X-ray techniques (Fig. S1-S4 in Supplementary materials).
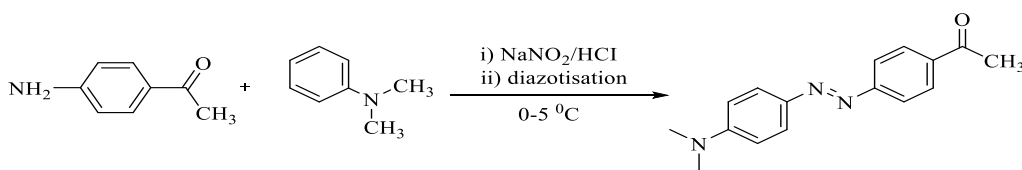
Scheme 2. *Synthetic pathway of DMA.*

2.3. Preparation of (E)-1-(4-((4-(phenylamino)phenyl)diazenyl)phenyl)ethanone

2.0 mmol (0.27 g) of 4-aminoacetophenone was dissolved in hydrochloric acid (1.5 mL conc. HCl in 4 mL water). Sodium nitrite (0.15 g, 2.0 mmol) in water (3 mL) was gradually added to this solution over 15 min. period at temperature range of 0-5 °C while stirring. The reaction mixture was stirred for 30 min. at temprature range of 0-5 °C. Excess nitrous acid was destroyed by the addition of urea. 4-*N,N*-dimethylaniline (2.0 mmol, 0.34 g) was dissolved in acetic acid/propionic acid (4-6 mL, ratio 3:1) and cooled to temprature range of 0-5 °C in a salt/ice bath. The cold diazonium salt solution was added to this cooled solution over for 1 hour with vigorous stirring in a drop-wise manner, while maintaining the pH between 4-6 by the addition of saturated sodiumcarbonate solution. The mixture was further stirred for 1 hour at temprature range of 0-5 °C and the resulting solid was filtered, washed with cold water, dried, and crystallized from ethanol as red crystals (yield: 0.37 g, 69%; m.p: 201-202 °C); FT-IR (ATR, υ$_{max.}$, cm^{-1}): 1670 (C=O), 1587 (aromatic C=C); ^{1}H-NMR (DMSO-d_6, 300 MHz): δ$_H$ 8.1 (d , *J* = 8.43 Hz, 2H), 7.90-7.80 (m, 4H), 6.83 (d, *J* = 8.90 Hz, 2H), 3.10 (s, 6H, N(CH$_3$)$_2$), 2.60 (s, 3H) ppm;^{13}C-NMR (DMSO-d_6, 75

MHz): δ_C 197.7, 155.4, 153.4, 148.2, 143.1, 137.1, 130.9, 129.9, 125.7, 122.2, 118.0, 112.0, 29.5, 27.2 ppm; LC-MS (ESI, CH_3CN, M+H)$^+$ ($C_{20}H_{18}N_3O$) found: 268.16, calcd.: 268.14.

2.4. X-ray crystal structure analysis

The solid-state structure of DMA was confirmed by X-ray diffraction analysis. Data were obtained with Bruker SMART BREEZE CCD diffractometer. The graphite-monochromatized Mo K_α radiation (λ=0.71073 Å) and oscillation scans technique with $\Delta\omega$=5° for one image were used for data collection. The lattice parameters were determined by the least-squares methods on the basis of all reflections with $F^2 > 2\sigma(F^2)$. Integration of the intensities, correction for Lorentz and polarization effects and cell refinement was performed using 'Bruker SAINT' and 'Bruker APEX2' software programs [27]. The structures were solved by direct methods using SHELXS-97 [28] and refined by a full-matrix least-squares procedure using the program SHELXL-97 [28]. H atoms were positioned geometrically and refined using a riding model. The final difference Fourier maps showed no peaks of chemical significance. The important conditions for the data collection and the structure refinement parameters of DMA are given in Table 1.

Table 1. *Crystal data and structure refinement for DMA.*

|	
Empirical formula	$C_{16}H_{17}N_3O$
Formula weight	267.33
Temperature	293(2) K
Wavelength	0.71073 Å
Crystal system	monoclinic
Space group	*P2₁/c*
Unit cell dimensions	a = 9.8234(5) Å $\quad \alpha$ =90°
	b =6.1735(3) Å β =98.619(2)°
	c =23.1178(11) Å $\quad \gamma$=90°
Volume	1386.14(12) Å^3
Z	4
Density (calculated)	1.281 Mg / m^3
Absorption coefficient	0.083 mm^{-1}
F(000)	568
θ range for data collection	1.7– 28.4°
Index ranges	$-13 \leq h \leq 13$, $-8 \leq k \leq 8$, $-30 \leq l \leq 30$
Reflections collected	25009
Independent reflections	3474 [R_{int} = 0.040]
Completeness to θ = 28.50°	99.5 %
Refinement method	Full-matrix least-squares on F^2
Data / restraints / parameters	2717 / 0 / 184
Goodness-of-fit on F^2	1.097
Final R indices [$F^2 > 2\sigma(F^2)$]	$R1$ = 0.0703, $wR2$ = 0.176
R indices (all data)	$R1$ = 0.088, $wR2$ = 0.189
Largest diff. peak and hole	0.260 and −0.250 Å^{-3}

3. COMPUTATIONAL DETAILS

Gaussian 09 program package [29] was used to optimize geometry and to provide information on the structural features of DMA. The initial geometries were taken from X-ray data. Ground state geometry of the molecule in gas and various solvents was optimized using DFT and HF methods with 6-31+G(d,p) basis set. In DFT calculations, the Becke's three parameter exchange functional (B3) [30] combining with nonlocal correlation functional by Lee, Yang and Parr (LYP) [31] was used. The vertical excitation energies and oscillator strengths at the optimized ground state equilibrium geometries were obtained using TD-DFT. All the computations in solvents with different polarities were carried out using the Self-Consistent Reaction Field (SCRF) under the Polarizable Continuum Model (PCM) [32]. In order to get further data for the structure of DMA, the ^{1}H and ^{13}C-NMR chemical shifts were obtained by DFT GIAO [32] model at B3LYP/6-31+G(d,p) level. The first-order hyperpolarizability (β_0) and related properties (μ and α_0) of the molecule were calculated by using and DFT/6-31+G(d,p) and HF/6-31+G(d,p) methods.

4. RESULTS AND DISCUSSION

4.1. Structural description

The molecular structure of DMA with atom-numbering scheme is shown in Fig.1. It crystallizes in the monoclinic P21/c space group without the presence of any solvent molecule. The molecule contains the azo group linking two aromatic rings to each other. The bond length of the azo unit (N1-N2) is 1.257Å, indicative of the typical double-bond character. The crystallographic results of the bond lengths N2-C7 and N1-C3 are 1.408 Å and 1.426 Å, respectively. The bond angles between aryl and azo groups are 113.5°for (N2-N1-C3) and 114.9° for (N1-N2-C7). The molecule is nearly planar and its phenyl rings attached to azo group has *trans*-isomer conformation.

Furthermore, weak intermolecular C-H…O hydrogen bonding interactions are found between the dimethylamine hydrogen atoms and its adjacent carbonyl oxygen atom O4 (C14-H…O4=3.562Å, C15-H…O4=3.602Å). Thus a head-to-tail dimeric packing fashion between adjacent planar molecules in its crystal structure is also observed. Nevertheless, the aromatic rings between adjacent planar dimeric units are severely offset and no π-π stacking interactions was found.

(a)

(b)
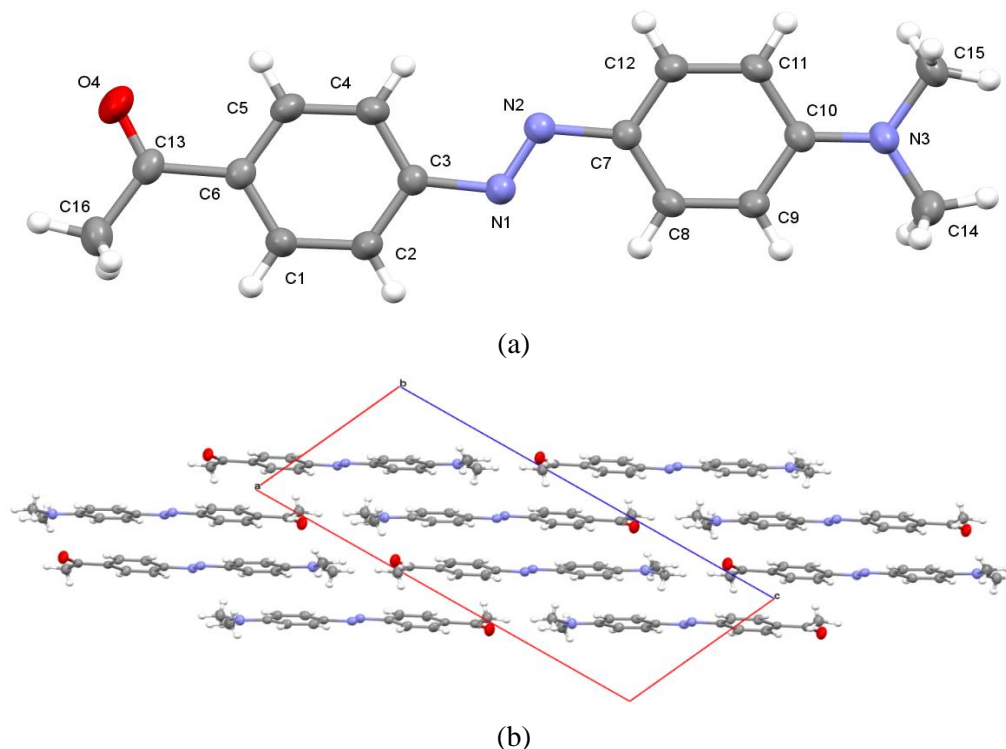
Figure 1. *(a) Molecular diagram of DMA with the thermal ellipsoids at the 50% probability level. (b) Molecular stacking of DMA with the unit cell viewed down along the b-axis.*

4.2. Molecular geometry

Initial geometry generated from the X-ray results was optimized without any constraint at Hartree–Fock and B3LYP levels using 6-31+G(d,p) basis set. For both of calculation levels, the optimized structural parameters were used in the vibrational frequency calculations to characterize all the stationary points as minima. The optimized molecular structure of the molecule is shown in Fig. 2.
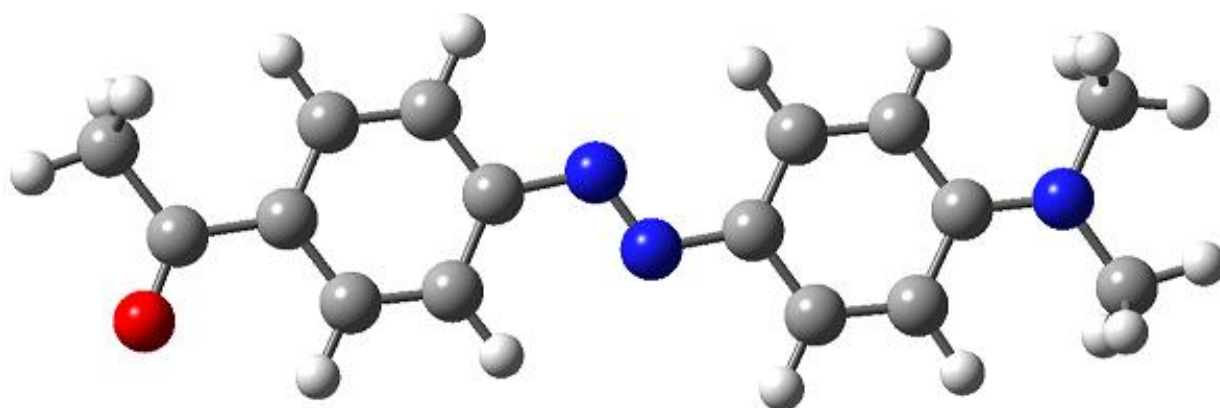
Figure 2. *The optimized molecular structure of DMA using B3LYP/6-31+G(d,p).*

The optimization geometrical parameters obtained by the HF and DFT/B3LYP are shown in Table 2 with the X-ray results, which are in accordance with the atom numbering scheme given in Fig. 1.

Table 2. *Some selected geometrical parameters of DMA.*

	exp.	calc.			exp.	calc.	
		DFT	HF			DFT	HF
Bond lengths(Å)				*Bond angles (°)*			
N2 N1	1.256(2)	1.266	1.221	N1 N2 C7	114.92(15)	115.95	116.65
N2 C7	1.408(2)	1.400	1.409	N2 N1 C3	113.53(15)	114.69	115.39
N1 C3	1.426(2)	1.416	1.421	N3 C10 C11	121.57(16)	121.37	121.50
C10 N3	1.366(2)	1.376	1.371	N3 C10 C9	120.99(16)	121.09	121.15
C10 C11	1.407(2)	1.419	1.404	C11 C10 C9	117.44(15)	117.53	117.35
C10 C9	1.409(2)	1.425	1.412	C1 C6 C5	118.40(15)	118.74	118.89
C6 C1	1.383(2)	1.405	1.389	C5 C6 C13	118.50(16)	118.69	118.53
C6 C5	1.391(3)	1.410	1.398	C9 C8 C7	120.89(16)	120.76	120.74
C6 C13	1.495(2)	1.497	1.500	C4 C3 N1	124.17(16)	125.02	124.55
C8 C9	1.368(2)	1.383	1.376	O4 C13 C16	120.58(17)	120.15	120.45
C8 C7	1.394(2)	1.411	1.394	C10 N3 C15	120.97(16)	120.13	120.11
C3 C2	1.379(3)	1.403	1.385	C12 C7 N2	116.59(15)	116.26	116.48
C3 C4	1.388(2)	1.410	1.396	*Torsion angles(°)*			
C13 O4	1.216(2)	1.226	1.197	C7 N2 N1 C3	-178.78(14)	-180.00	-180.00
C13 C16	1.494(3)	1.520	1.513	N2 N1 C3 C2	-173.77(17)	179.99	179.99

N3 C14	1.446(3)	1.456	1.447	N2 N1 C3 C4	8.0(3)	-0.01	-0.01
N3 C15	1.446(2)	1.456	1.446	C1 C6 C13 O4	-177.43(19)	179.99	179.99
C12 C11	1.375(2)	1.387	1.382	C1 C6 C13 C16	2.2(3)	0.00	0.00
C12 C7	1.389(2)	1.405	1.386	C11 C10 N3 C14	179.18(18)	179.99	179.99
C1 C2	1.386(2)	1.393	1.388	C9 C10 N3 C14	-1.0(3)	-0.01	-0.01
C5 C4	1.374(3)	1.386	1.378	C11 C12 C7 N2	-178.52(16)	179.99	-180.00
				N1 N2 C7 C12	176.35(16)	-180.00	180.00
				N1 N2 C7 C8	-3.3(3)	0.00	0.00

The optimized bond lengths of C-C in the phenyl ring1 and phenyl ring 2 (N-CH3) fall in the range 1.378-1.398 Å and 1.376-1.412 Å for HF/6-31+G(d,p) and 1.393-1.410 Å and 1.383-1.425 Å for B3LYP/6-31+G(d,p) method, which are in good agreement with experimental results, 1.379-1.391 Å and 1.375-1.409 Å, respectively. The N1-C3 and N2-C7 bond lengths are 1.421 Å and 1.409 Å for HF and 1.416 Å and 1.400 Å for B3LYP methods, which are 1.426 Å and 1.408 Å for X-ray results, respectively. According to the X-ray results N-N bond length is 1.256 Å and the optimized lengths are 1.221 Å for HF and 1.266 Å for B3LYP which are in agreement with X-ray results (Table 2). The geometry of the molecule is planar with the obtained value of C3–N1–N2–C7 is -180.0° from calculations and -178.78° from the X-ray structure analysis. The calculated torsion angles N2–N1–C3–C2 and N1–N2–C2–C12 are 179.99° for HF and B3LYP and the corresponding experimental torsion angles obtained from the X-ray structure analysis are -173.77°.

4.3. Photophysical properties

The absorption spectra were recorded over the range of 300-700 nm using a variety of solvents in concentrations 30 μM. The experimental and theoretical absorption wavelengths were obtained in various solvents having different dielectric constants (ε) such as DMSO (ε=46.7), DMF (ε=36.7), methanol (ε=32.7), THF (ε=7.58), Acetic acid (ε=6.15), Chloroform (ε=4.81) and Toluene (ε=2.38). In the calculations, the absorption spectra of DMA were obtained at the optimized structure of the ground state in each solvents using the PCM model linked to TD-DFT (B3LYP) with the 6-31+G(d,p). The computed values of absorption wavelength (λ_{max}), oscillator strength (*f*) and orbital contribution as well as the experimental data of DMA are shown in Table 3.

Table 3. *Experimental and theoretical electronic absorption spectra values in different solvents of DMA.*

| Solvents	Experimental		Computed (TD-DFT)		
	λ_{max} (nm)	Molar absorptivity	λ_{max} (nm)	Oscillator strength	Orbital contribution
Gas phase	-	-	428	1.059	H→L
DMSO	460	4.22	479	1.193	H→L
DMF	453	4.30	479	1.196	H→L
Methanol	444	4.11	475	1.169	H→L
THF	440	4.45	473	1.191	H→L
Acetic acid	455	4.16	471	1.183	H→L
Chloroform	445(555s)	4.18	472	1.248	H→L
Toluene	437	4.09	465	1.215	H→L

s=shoulder

The absorption spectra of the molecule has only one absorption maximum in all solvents used, except in Chloroform. However, the positive solvatochromic properties are seen in all solvents, i.e. there is a

bathochromic shift of the absorption band with increasing solvent polarity. The electronic absorption spectra of the molecule shows shorter wavelength absorption maxima in toluene at 437 nm (calc. 465 nm) and longer wavelength in DMSO at 460 nm (calc. 479 nm) (Table 3 and Fig. 3). This molecule consists of an electron-donating N,N-dimethylamine unit and electron-withdrawing acetyl group conjugated through π-bonding in both substituents. This behavior is typical of donor-acceptor π systems, in which an internal charge transfer occurs from donor to acceptor upon excitation. The polar excited state is stabilized by polar solvents such as DMSO and as a results, such a behavior could be observed. This observation is in agreement with previous work [25]. In addition, the existence of one absorption maxima with a shoulder in Chloroform is interpreted as a mixture of forms of the molecule in this solvent.
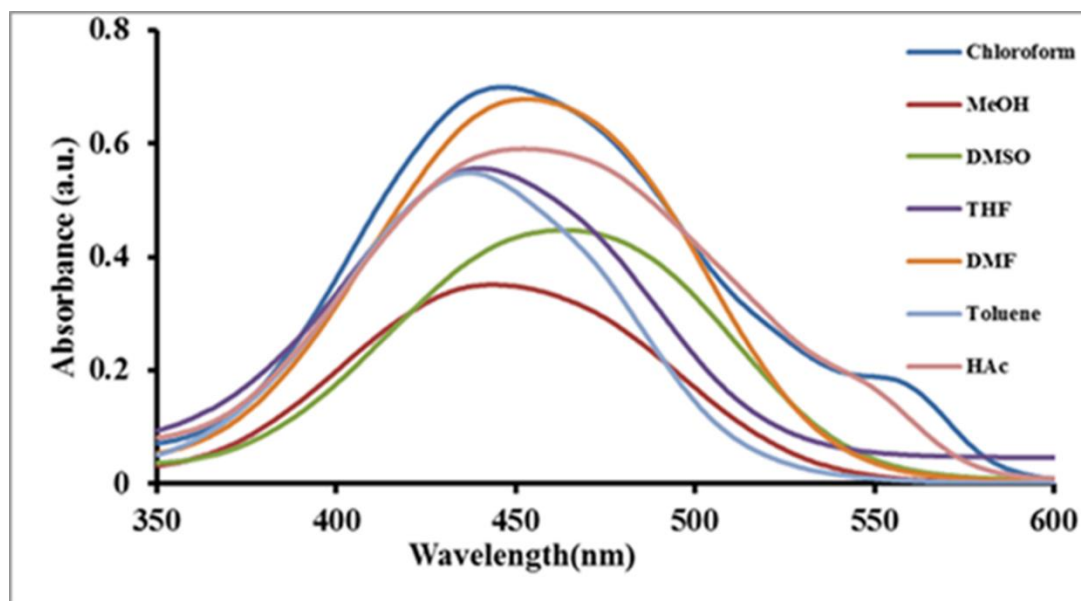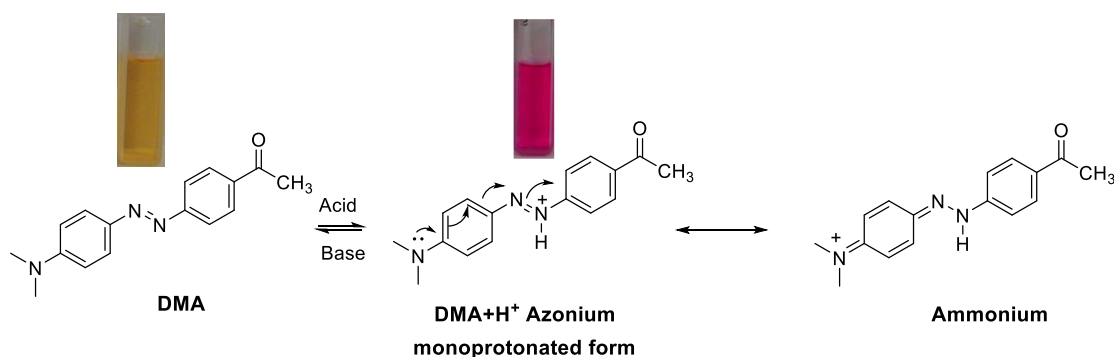

Figure 3. *Absorption spectra of DMA (c = 30 μM) in various solvents.*

The largest percentage deviation between the experimental and computed absorption maxima is 33 nm in THF and minimum deviation is 16 nm in Acetic acid. The electronic transition in each case includes HOMO-LUMO transition. The relevant HOMO and LUMO of the molecule for gas phase are shown in Fig.4. As one can see, the electron distribution in HOMO was largely located on donor N,N-dimethylaniline moiety and is moved to acceptor moiety through azo π-bridge after energy excitation. In the excitation from HOMO to LUMO, the charge transfer takes place from donor N,N-dimethylaniline moiety to the acceptor end.
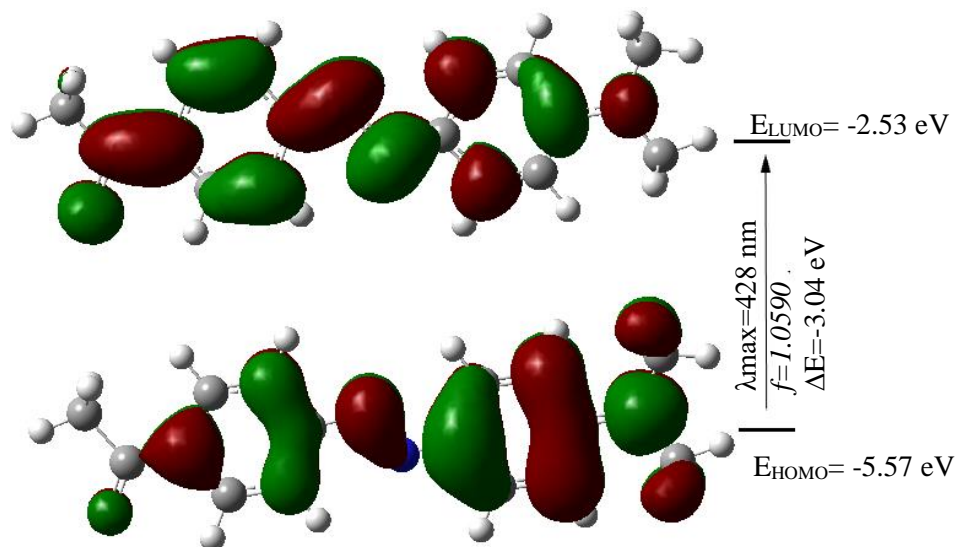
Figure 4. *The frontier molecular orbitals of DMA in the gas phase.*

The determination and monitoring of pH change is quite important especially for cellular system. In our previous studies, it was shown that nitrogen atoms in azo bridge have protonation possibility. Therefore, the halochromic effect of DMA was also investigated with addition trifluoroacetic acid (TFA in Chloroform) to solution of dye in Chloroform. The change in the UV-vis absorption spectra of DMA upon addition of acid is illustrated in Fig. 5. Upon addition of TFA to a solution of DMA in Chloroform, it exhibited major color changes from yellow to red with the growth of a new absorption bands at 525 and 552 nm respectively and a well-defined isosbestic point at ca. 474 nm (Fig. 5 and Scheme 3).


Scheme 3. *Prototropic equilibria of DMA in Chloroform.*
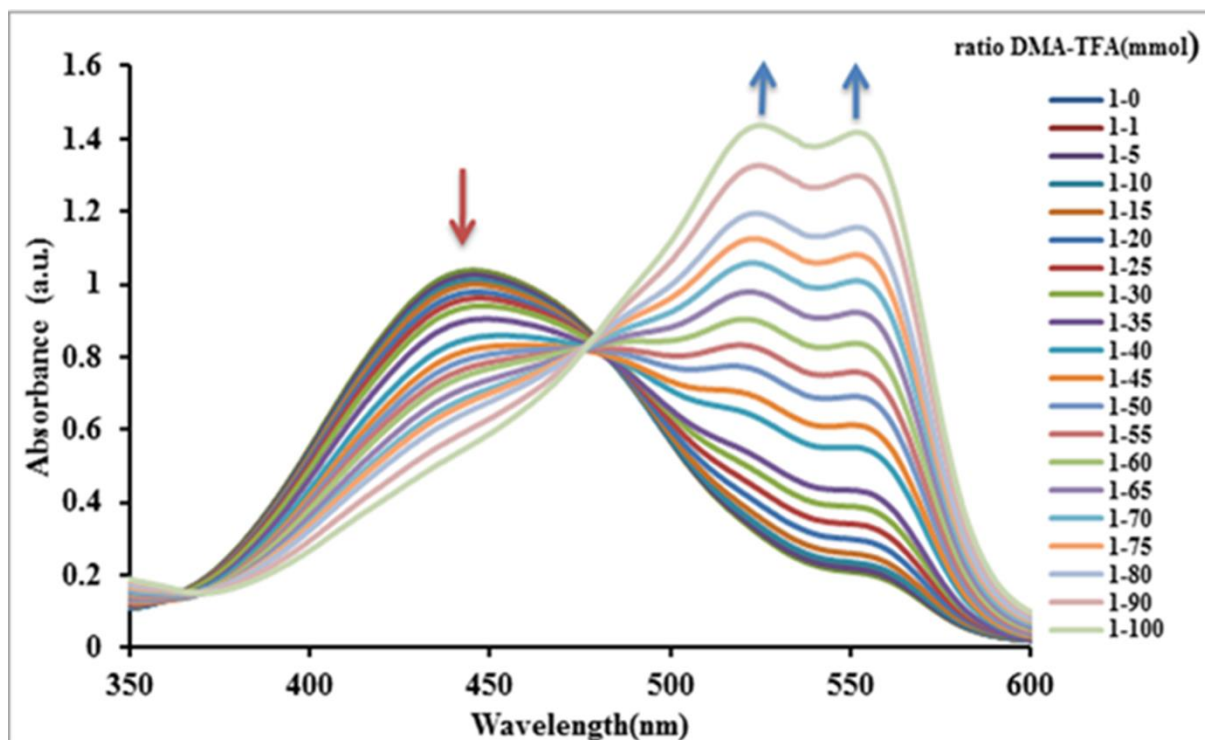
Figure 5. *The absorption spectra of DMA (c = 30 μM) upon addition of TFA (1 M) in Chloroform.*

According to this results, there is a ground-state equilibrium between neutral (DMA) and monoprotonated (DMA+H$^+$) species. The observed two absorption maxima in UV-vis spectra showed that DMA+H$^+$ may be stable as azonium or ammonium forms. In both forms, the positive charge on β-nitrogen and N,N-dimethylamino functionality is completely delocalized and bathochromic shift (about 117 nm) with respect to the neutral form is observed experimentally. These results point out that it can be used as potential pH chemosensor for acidic medium. However, if pH sensor has reversibility to pH change it is more usable for industrial applications. To test the reversibility of DMA chemosensor, we determined changing in absorption spectrum after the addition of piperidine in solution of DMA+H$^+$. The spectral change in absorption spectrum of DMA+H$^+$ with the addition of piperidine in chloroform solution is shown in Fig.6. In Chloroform, the absorption bands at 525 and 552 nm disappeared and a new absorption maximum at the same absorption maximum of the neutral form (432 nm) was observed as illustrated in Fig. 6.
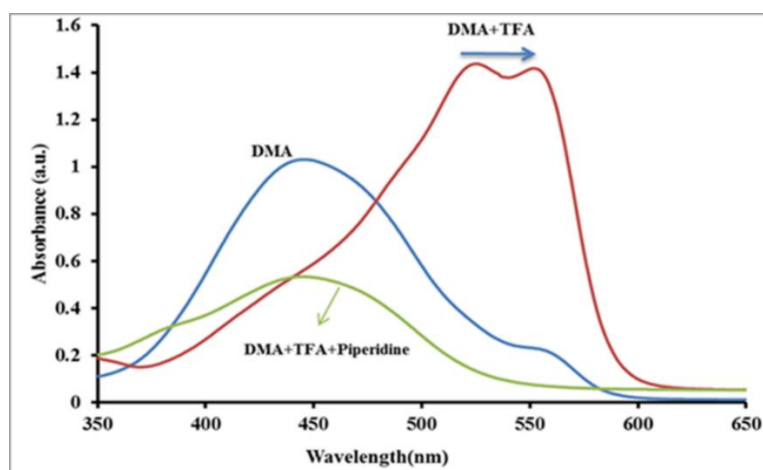
Figure 6. *Absorption spectra of DMA (c = 30 μM) in the presence of TFA (1 M) and upon addition of increasing amounts of piperidine in Chloroform.*

4.4. NMR spectra

Experimental and theoretical values of ^{1}H and ^{13}C-NMR chemical shifts of DMA together with the corresponding experimental values with the numbering in Fig.1 are shown in Table 4. The ^{1}H and ^{13}C chemical shifts were estimated by using the corresponding tetramethylsilane (TMS) shielding calculated in advance at the same theoretical level as the reference. Calculated ^{1}H and ^{13}C isotropic chemical shielding for TMS were 31.64 ppm and 193.14 ppm at B3LYP/6-31+G(d,p) level, 32.26 ppm and 203.68 ppm at the HF/6-31+G(d,p) level in DMSO, respectively.

It is found that the aromatic protons were observed at 6.8-8.1 ppm in the ^{1}H-NMR spectra measured in DMSO-d_6, whereas the calculated values are appeared at 6.9-8.5 ppm and 7.0-8.9 ppm by B3LYP and HF, respectively. Aliphatic protons appeared at 3.10 ppm for $-N(CH_3)_2$ and 2.60 ppm for $-COCH_3$ as singlet experimentally. These chemical shifts theoretically predict at 3.2 ppm and 3.1 ppm for $-N(CH_3)_2$ and 2.7 ppm for $-COCH_3$ at B3LYP and HF levels of theory, respectively. On the other hand, the ^{13}C-NMR spectra measured in DMSO-d_6 showed peaks in the range of 27.2-197.7 ppm while the calculation results were observed in the range of 28.4-194.8 ppm and 27.2 94.7 ppm by B3LYP and HF, respectively. The largest deviations between the calculated and experimental ^{13}C-NMR chemical shifts observed for C4 with 15.4 and for C12 with 18.1 ppm by B3LYP and HF, respectively.

Table 4. *Experimental and calculated ^{1}H and ^{13}C-NMR chemical shifts (ppm) of DMA.*

Atom no.	exp.	B3LYP	HF	Atom no.	exp.	B3LYP	HF
H1	8.1	8.4	8.8	C1	130.9	130.7	134.4
H2	7.8-7.9	8.1	8.7	C2	125.7	128.8	129.5
H4	7.8-7.9	8.3	8.6	C3	155.4	153.9	154.7
H5	8.1	8.5	8.9	C4	125.7	110.3	112.9
H8	7.8-7.9	8.3	8.9	C5	130.9	126.8	131.0
H9	6.8	6.9	7.0	C6	143.1	131.9	135.1
H11	6.8	6.9	7.0	C7	153.4	142.6	137.2
H12	7.8-7.9	8.0	8.9	C8	122.2	113.3	121.0
H14	3.0	3.2	3.1	C9	118.0	110.4	107.4
H15	3.0	3.2	3.1	C10	148.2	149.6	157.0
H16	2.6	2.7	2.7	C11	118.0	109.1	106.0
				C12	122.2	134.4	140.3
				C13	197.7	194.8	194.7
				C14	-	41.6	37.6
				C15	-	41.9	37.7
				C16	27.2	28.4	27.2

4.5. Nonlinear optical properties (NLO)

It is known that the DFT [34, 35] calculations for the prediction of the NLO properties of the molecules provides clearly improved accuracy with respect to HF calculations. Nevertheless, in the present study, the NLO properties of the studied molecule have been investigated using HF and DFT methods to compare the results and to provide the insight for the literature.

The dipole moment (μ), polarizability (α_{tot}) and first hyperpolarizability (β_{tot}) values of DBG calculated by HF and B3LYP methods at 6-31+G(d,p) level were given in Table 5. The dipole moment (μ), the polarizability (α_{tot}) and the first hyperpolarizability (β_{tot}) for the studied compound are defined as follows:

$\mu = (\mu_x{}^2 + \mu_y{}^2 + \mu_z{}^2)^{1/2}$,

$\alpha_{tot} = 1/3\,(\alpha_{xx} + \alpha_{yy} + \alpha_{zz})$,

$\beta_{tot} = (\beta_x + \beta_y + \beta_z)^{1/2}$,

where β_i is defined as:

$\beta_i = (\beta_{iii} + \beta_{ijj} + \beta_{ikk})$ i, j, k = x, y, z.

As seen in Table 5, the β_x value dominates the second-order NLO response as a result of situation of the skeleton atoms on the x-axis. The β_y value also provides a small contribution to the second-order NLO responses whereas the β_x value is close to zero. It is clearly seen that the HF and DFT results display the same trend in β compounds. For all that, the calculated β_{tot} is 41.3×10^{-30} esu and 132.6×10^{-30} esu for HF and DFT methods, respectively. The first hyperpolarizability value of urea used as a ptototypical molecules in the study of the NLO systems was computed using DFT/B3LY/6-31+G(d,p) method as 0.49×10^{-30} esu. According to these results, the β value of present molecule is more than 270 times larger than the magnitude of urea and the molecule can obtain a good NLO candidate.

Table 5. *The electric dipole moment (μ), the polarizability (α) and the first hyperpolarizability (β$_{tot}$) and their components calculated by HF and DFT at 6-31+g(d,p) level for DMA.*

DFT				HF			
μ&α		*β*		*μ & α*		*β*	
α_{xx}	570.325	β_{xxx}	15788.471	α_{xx}	389.471	β_{xxx}	5084.938
α_{xy}	2.735	β_{xxy}	-388.044	α_{xy}	4.948	β_{xxy}	-159.984
α_{yy}	207.183	β_{xyy}	-347.585	α_{yy}	191.627	β_{xyy}	-275.049
α_{xz}	-0.009	β_{yyy}	65.879	α_{xz}	-0.003	β_{yyy}	28.899
α_{yz}	0.004	β_{xxz}	-0.232	α_{yz}	0.003	β_{xxz}	0.576
α_{zz}	120.235	β_{xyz}	-0.360	α_{zz}	115.651	β_{xyz}	0.319
α (esu)	44.3×10^{-24}	β_{yyz}	0.065	*α*	34.4×10^{-24}	β_{yyz}	-0.031
μ_x	-3.007	β_{xzz}	-96.963	μ_x	-2.226	β_{xzz}	-31.502
μ_y	1.092	β_{yzz}	25.697	μ_y	1.141	β_{yzz}	18.746
μ_z	0.000	β_{zzz}	0.031	μ_z	0.000	β_{zzz}	-0.077
μ (D)	8.133	β_x*(esu)*	132.6×10^{-30}	*μ (D)*	6.358	β_x*(esu)*	41.3×10^{-30}
		β_y*(esu)*	-2.56×10^{-30}			β_y*(esu)*	-0.97×10^{-30}
		β_z*(esu)*	-1.18×10^{-33}			β_z*(esu)*	4.04×10^{-33}
		β (esu)	132.6×10^{-30}			*β(esu)*	41.3×10^{-30}

4.6. Thermal Stability

Thermal stability of DMA was investigated by using thermo-gravimetric analysis (TGA) in the temperature range 0-600 °C under nitrogen gas at a heating rate of 10 °C min^{-1}. The change in weight of the compounds was measured as a function of temperature. Thermal stability of the dye is shown in Fig.7. The solids have no water molecule because the compounds did not loss up weight to 100 °C. The TGA results indicate that DMA is stable up to 235 °C. The Td value showed that the compound is enough for industrial applications field using as textile and optic dye.
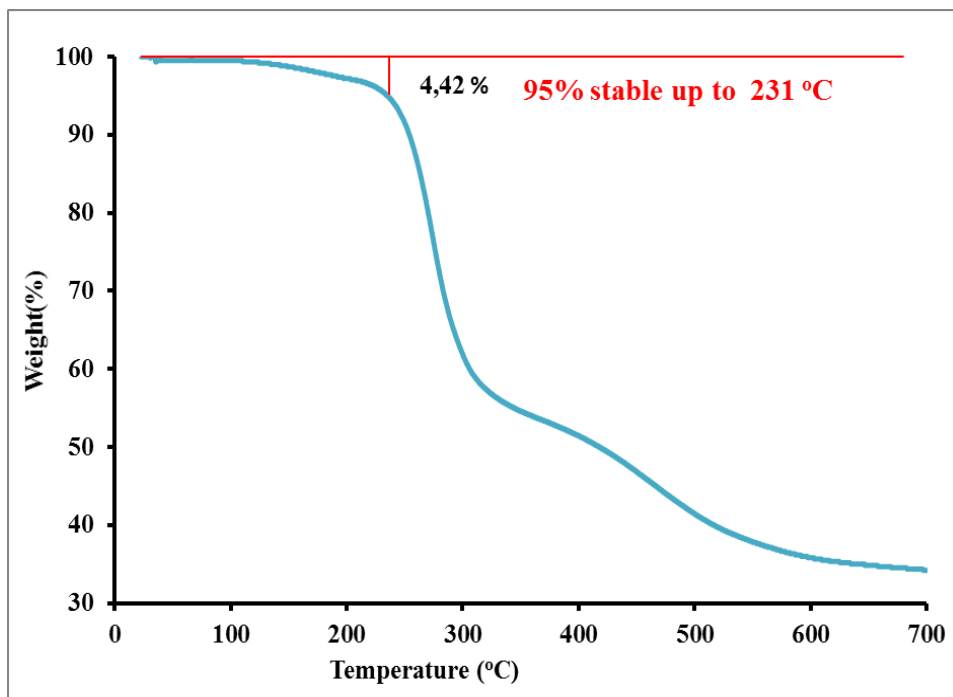
Figure 7. *TGA curve of DMA.*

5. CONCLUSION

In this study, we synthesized dimethylaniline based azo disperse dye under simple reaction conditions using azo coupling and characterized by x-ray diffraction, UV-vis, FT-IR, ^{1}H/^{13}C-NMR, thermal analysis, mass spectroscopic techniques, and DFT calculations. The solvent effects on the visible absorption spectra of the synthesized molecule were evaluated. The synthesized azo dye showed single bands in UV-vis absorption spectra in all solvents used except chloroform. Moreover, it shows halochromic behavior after addition of TFA in Chloroform and the color change from yellow to red was seen in solvent used with acidification. In addition, the absorption curves of the molecule are very sensitive to acidic solution leading to bathochromic shift. The obtained results show that the molecule possesses a good thermal stability and was a good NLO candidate. It can be applied to polyester and/or polyamide fibers as disperse dye and also is good candidate for optic application.

ACKNOWLEDGEMENTS

SUPPLEMENTARY MATERIAL

Supplementary data (copies of IR, ^{1}H-NMR, ^{13}C-NMR, and LC-MS spectra for dye Figs. S1–S4) associated with this article can be found, in the online version, at … CCDC-1409412 contains the supplementary crystallographic data for this structure (DMA). These data can be obtained free of charge via ww.ccdc.cam.ac.uk/conts/retrieving.html (or from the Cambridge Crystallographic Data Centre, 12 Union Road, Cambridge CB2 1EZ, UK; fax: (+44) 1223 336 033; or deposit@ccdc.ca.ac.uk)

CONFLICT OF INTEREST

No conflict of interest was declared by the authors

REFERENCES

[1] Zollinger, H., Color Chemistry, Synthesis, Properties and Applications of Organic Dyes and Pigments 3th ed., Wiley-VCH, (2003).

[2] Hunger, K., Industrial Dyes, Chemistry, Properties, Applications 2nd ed., WILEY-VCH Verlag GmbH & Co. KgaA, Weinheim, (2003).

[3] Berber, H., Ogretir, C., Lekesiz E.C.S., Ermis, E., "Spectroscopic Determination of Acidity Constants of Some Monoazo Resorcinol Derivatives", J. Chem. Eng. Data, 53: 1049–1055, (2008).

[4] Koh, J., Kim, S., Kim, J.P., "Synthesis and spectral properties of azohydroxypyridone disperse dyes containing a fluorosulphonyl group", Color. Technol., 120: 241–246, (2004).

[5] Umape, P.G., Patil, V.S., Padalkar, V.S., Phatangare, K.R., Gupta, V.D., Thate, A.B., Sekar, N., "Synthesis and characterization of novel yellow azo dyes from 2-morpholin-4-yl-1,3-thiazol-4(5H)-one and study of their azo-hydrazone tautomerism", Dyes Pigments, 99: 291–298, (2013).

[6] Ferraz, E.R.A., Oliveira, G.A.R., Grando, M.D., Lizier, T.M., Zanoni, M.V.B., Oliveira, D., "Photoelectrocatalysis based on Ti/TiO2 nanotubes removes toxic properties of the azo dyes Disperse Red 1, Disperse Red 13 and Disperse Orange 1 from aqueous chloride samples", J. Environ. Manage., 124: 108–114, (2013).

[7] Bushuyev, O.S., Singleton, T.A., Barrett C.J., "Fast, Reversible, and General Photomechanical Motion in Single Crystals of Various Azo Compounds Using Visible Light", Adv. Mater., 25: 1796–1800, (2013).

[8] Henzl, J., Boom, K., Morgenstern, K., "Using the First Steps of Hydration for the Determination of Molecular Conformation of a Single Molecule", J. Am. Chem. Soc.,136: 13341−13347, (2014).

[9] Uliana, C.V., Garbellini, G.S., Yamanaka, H., "Electrochemical investigations on the capacity of flavonoids to protect DNA against damage caused by textile disperse dyes", Sens. Actuators B: Chem., 192: 188–195, (2014).

[10] Blumberg, S., Martin, S.F., "4-(Phenylazo)diphenylamine (PDA): a universal indicator for the colorimetric titration of strong bases, Lewis acids, and hydride reducing agents.", Tetrahedron Lett., 56: 3674–3678, (2015).

[11] Seclaman, E., Sallo, A., Elenes, F., Crasmareanu, C., Wikete, C., Timofei, S., Simon, Z., "Hydrophobicity, protolytic equilibrium and chromatographic behaviour of some monoazoic dyes", Dyes Pigments, 55: 69–77(2002).

[12] Towns A.D., "Developments in azo disperse dyes derived from heterocyclic diazo components", Dyes Pigments, 42: 3–28, (1999).

[13] Chao, Y.C., Lin, S.M., "Carboxy-substituted monoazo dyes for wool-polyester blends", Dyes Pigments, 44: 209–218, (2000).

[14] Ferraz, E.R.A, Oliveira, G.A.R., Grando, M.D., Lizier, T.M., Zanoni, M.V.B., Oliveira D.P., "Photoelectrocatalysis based on Ti/TiO2 nanotubes removes toxic properties of the azo dyes Disperse Red 1, Disperse Red 13 and Disperse Orange 1 from aqueous chloride samples", J. Environ. Manage., 124: 108–114, (2013).

[15] Uliana, C.V., Garbellini, G.S., Yamanaka, H., "Evaluation of the interactions of DNA with the textile dyes Disperse Orange 1 and Disperse Red 1 and their electrolysis products using an electrochemical biosensor", Sens. Actuators B: Chem., 178: 627–635, (2013).

[16]Miao S., Zhu Y., Zhuang, H., Xu, X., Li, H., Sun, R., Li, N., Ji, S., Lu, J., "Adjustment of charge trap number and depth in molecular backbone to achieve tunable multilevel data storage performance", J. Mater. Chem. C, 1: 2320–2327 (2013).

[17]Zhuang H., Zhang, Q., Zhu, Y., Xu, X., Liu, H., Najun, L., Xu, Q., Li, H., Lu, J., Wang, L., "Effects of terminal electron acceptor strength on film morphology and ternary memory performance of triphenylamine donor based devices", J. Mater. Chem. C: 1 3816–3824, (2013).

[18]Mourot, A., Kienzler, M.A., Banghart, M.R., Fehrentz, T., Huber, F.M.E., Stein, M., Kramer, R.H., Trauner, D., "Tuning Photochromic Ion Channel Blockers", ACS Chem. Neurosci., 2: 536–543 (2011).

[19]Carolina V., Uliana, G.S., Yamanaka, G.H., "Electrochemical reduction of Disperse Orange 1 textile dye at a boron-doped diamond electrode", J. Appl. Electrochem., 42: 297–304, (2012).

[20]Shin, D.M., Shanzea, K.Z., Whitten, D.G., "Solubilization Sites and Orientations in Microheterogeneous Media. Studies Using Donor-Acceptor-Substituted Azobenzenes and Bichromophoric Solvatochromic Molecules", J. Am. Chem. Soc., 111: 8494–8501, (1989).

[21]Ishow, E., Bellaiche, C., Bouteiller, L., Nakatani, K., Delaire, J.A., "Versatile Synthesis of Small NLO-Active Molecules Forming Amorphous Materials with Spontaneous Second-Order NLO Response", J. Am. Chem. Soc., 125: 15744–15745, (2003).

[22]Babür, B., Seferoglu, N., Aktan, E., Hökelek, T., Sahin, E., Seferoglu, Z., "Phenylazoindole dyes 3: Determination of azo-hydrazone tautomers of new phenylazoindole dyes in solution and solid state", J. Mol. Struct.,1081: 175–181, (2015).

[23]Aktan, E., Babür, B., Seferoğlu, Z., Hökelek, T., Şahin, E., "Synthesis and structure of a novel hetarylazoindole dye studied by X-ray diffraction, FT-IR, FT-Raman, UV–vis, NMR spectra and DFT calculations", J. Mol. Struct., 1002: 113–120, (2011).

[24]Babür, B., Seferoglu, N., Aktan, E., Hökelek, T., Sahin, E., Seferoglu, Z., "Phenylazoindole dyes 2: The molecular structure characterizations of new phenylazo indoles derived from 1,2-dimethylindole", Dyes Pigments, 103: 62–70, (2014).

[25]Aksungur, T., Arslan, Ö., Seferoglu, N., Seferoglu, Z., "Photophysical and theoretical studies on newly synthesized N,N-diphenylamine based azo dye", J. Mol. Struct., 1099: 543–550, (2015).

[26] Lin, L. R., Wang X., Wei, G.N., Tang, H. H., Zhanga, H., and Ma, L. H.," Azobenzene- derived tris-β-diketonate lanthanide complexes: reversible trans-to-cisphotoisomerization in solution and solid state", Dalton Trans., 45:14954-14964, (2016).

[27]Bruker, 'Bruker SAINT' and 'Bruker APEX2' software programs. Bruker AXS Inc., Madison, Wisconsin, USA(2007).

[28]Sheldrick, G.M., SHELXS97 and SHELXL97, University of Göttingen, Germany, (1997).

[29]Frisch, M.J., Trucks, G.W., Schlegel, H.B., Scuseria, G.E., Robb, M.A., Cheeseman, J.R., et al. Gaussian 09, revision A.2. Wallingford CT: Gaussian, Inc. (2009).

[30]Becke, A.D., "A new mixing of HartreeeFock and local density-functional theories", J. Chem. Phys., 98: 1372–1377, (1993).

[31]Lee, C., Yang, W., Parr, R.G., "Development of the Colle-Salvetti correlation-energyformula into a functional of the electron density", Phys. Rev. B, 37: 785–789, (1988).

[32]Tomasi, J., Mennucci, B., Cammi, R., "Quantum mechanical continuum solvation models", Chem. Rev.105: 2999–3094, (2005).

[33]Wolinski, K., Hilton, J.F., Pulay, P., "Efficient Implementation of the Gauge-Independent Atomic Orbital Method for NMR Chemical Shift Calculations", J. Am. Chem. Soc. 112: 8251-8260, (1990).

[34]Hohenberg, P., Kohn, W., "Inhomogeneous Electron Gas", Phys. Rev., 136: B864, (1964).

[35]Kohn, W. and Sham, L. J., "Self-Consistent Equations Including Exchange and Correlation Effects", Phys. Rev. 140: A1133, (1965).